ION IMPLANTATION OF POLYMERS

M.S. DRESSELHAUS,[#*+] B. WASSERMAN,[#+] AND G.E. WNEK[#θ]
[*]Department of Electrical Engineering and Computer Science;
[#]Center for Materials Science and Engineering; [+]Department of Physics;
[θ]Department of Materials Science and Engineering;
Massachusetts Institute of Technology, Cambridge, MA 02139, USA

ABSTRACT

Ion implantation provides a mechanism for radically modifying the electronic and transport properties of a variety of polymers that are normally insulating. By using masks and tailoring the implanted species and ion energies, conducting paths in an insulating medium can be fabricated between specific reference points, an application of obvious relevance to the microelectronics industry. Specific results are reported for modification of the structure, electrical conductivity, thermoelectric-power, optical transmission and electron spin resonance for several polymers under a variety of implantation conditions. The temperature and frequency dependence of the conductivity suggest a one-dimensional variable range hopping mechanism for conduction along the polymer chains. Comparison is made between implantation in the 200 keV and 2 MeV energy ranges.

INTRODUCTION

Most polymeric materials can be regarded as good insulators and many have electrical resistivities of $> 10^{12}$ Ωcm. The electronic structure of these insulating polymers consists of saturated bonds and tangled and interrupted chains which result in few if any conduction mechanisms. The low cost and easy processibility of some polymers make them attractive as electronic materials. The general instability of chemically doped conducting polymers presents problems with regard to their practical utilization. In contrast, the alternate doping scheme by ion implantation produces stable conducting materials. However, the conducting mechanism for ion implanted polymers is more difficult to determine because of the physical damage associated with the implantation process. Extensive studies of ion implantation in graphite have been reported [1] and it is found that the extensively damaged graphite material bears many similarities to highly damaged ion-implanted polymeric materials with regard to their electrical properties and lattice modes [2].

Recent developments in microelectronics technology make extensive use of energetic beams of radiation (electron, x-ray, and ion) for patterning. Of significance is the higher sensitivity of the polymer (by ~2 orders of magnitude) to ion beams relative to electron beams, so that ion beam lithography is feasible at fluences of less than 10^{13}cm^{-2} [3]. For positive resists (e.g., PMMA), ion implantation results in scission of the molecular chains, while for negative resists (e.g., polystyrene), implantation results in crosslinking of polymer chains. In order to understand this technology in a more fundamental way, the investigation of radiation-induced defects in polymers has become an area of interest. The use of ion beams to define conducting paths (for example as interconnects) through an insulating polymer film has been demonstrated and is of potential interest in very large scale integrated circuit technology. Furthermore, microelectronic device structures have been applied to sensitively

Mat. Res. Soc. Symp. Proc. Vol. 27 (1984)
https://doi.org/10.1557/PROC-27-413 Published online by Cambridge University Press

measure transport properties of ion-implanted polymer films, using an interdigitated electrode configuration upon which a polymer film was spun and subsequently implanted using charge flow transitor technology [4,5].

A band-like conduction process has been discussed for the observed electronic properties of polyacetylene. Ion-implantation and chemical doping studies on polymers have been carried out on very disordered materials, so that a hopping process involving transitions between localized states forms the basis for any model of the electronic properties. Polymers typically have electronic band gaps $\geq$ 2 eV so that the localized states formed by the doping or implantation of polymers typically lie in this band gap. This paper focuses on the conduction mechanism in ion implanted polymers and on the nature of implantation-induced defects, including cross linking and scission of polymer chains, double bond, localized carrier and free radical formation and gas evolution.

ION IMPLANTATION AND SAMPLE CHARACTERIZATION

Ion implantation has been successfully applied to a number of normally insulating polymers to make them conducting, including the polymers poly(p-phenylene-sulfide) (PPS), poly(2,6-dimethylphenylene-oxide) (PPO), polyacrylonitrile (PAN) [4-6], poly(methyl methacrylate) (PMMA), poly(vinyl-chloride) (PVC) and other photoresists [2], and related non-polymeric organic thin films [7,8], 3,4,9,10-perylene-tetracarboxylic dianhydride (PTCDA), 1,4,5,8-napthalene-tetracarboxylic dianhydride (NTCDA), and Ni-phthalocyanine (NiPc). It has also been demonstrated that ion implantation can enhance the conductivity of polymers that are already conducting [9-11] such as polysulfurnitride $(SN)_x$ and polyacetylene $(CH)_x$. From this listing (see Fig. 1), it is seen that both simple chain (planar zig-zag) polymers and aromatic polymers with helical conformations can be rendered conducting by ion implantation.

Ion implantation studies on polymers are normally carried out on thin polymer films. These films are often prepared by dissolving the desired polymer in a solvent, which is then spun on to a substrate and heated to ~100°C to remove the solvent. Some solvents that have been used are: diphenyl ether or n-methyl-2-pyrrolidone for PPS [4,5]; chloroform for PPO [6]; and N,N dimethylformamide for PAN [6].

A wide range of ions have been implanted, including: ^{19}F, ^{36}Cl, ^{80}Br, ^{84}Kr, ^{127}I into PPS; ^{14}N and ^{80}Br into PPO; ^{14}N, ^{75}As, ^{80}Br, and ^{84}Kr into PAN; ^{4}He and ^{40}Ar into PTCDA, NTCDA and NiPc; ^{4}He and ^{40}Ar into PMMA and

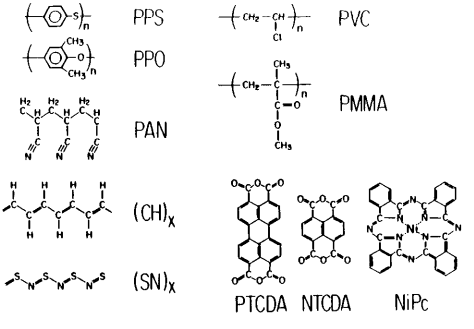

Fig. 1. Monomer units of polymers and related materials for which ion implantation has resulted in enhanced conduction.

https://doi.org/10.1557/PROC-27-413 Published online by Cambridge University Press

PVC; ^{80}Br and ^{106}Pd into $(SN)_x$; and ^{19}F, ^{36}Cl, ^{80}Br, ^{127}I into $(CH)_x$. Some workers [9-11] have used relatively low energy implants $25 < E < 90$ keV to confine the implants to near-surface regions of the polymer substrate, while other workers [4-6] have used intermediate ion energies $35 < E < 230$ keV and fluences ϕ in the range $3 \times 10^{14} < \phi < 5 \times 10^{16}$ cm^{-2}, and yet other workers [2,7,8] have used sufficiently high energy implants (E = 2 MeV) to completely penetrate the polymer films. Approximately uniform ion irradiation can be achieved in this case, since R_p for a 2 MeV $^4He^+$ ion exceeds 3μ, which is significantly larger than the film thickness of ~0.5 μ that was used [12]. The work in the various groups has not overlapped significantly either with respect to polymer substrate or ion energy range. In comparing the observed properties, consideration must be given to the difference in implantation conditions and choice of polymer films used by different workers.

The theory of implantation of ions in materials was originally developed for random or disordered solids [13]. In this form the theory is applicable to disordered polymeric materials with regard to the depth distribution of both the implanted ions and the structural damage. From this theory, a good estimate for the mean ion penetration depth R_p and the half width of the Gaussian distribution ΔR_p for ion implantation into bulk polymers can be obtained by assuming the density of the polymer to be that of amorphous carbon. Typical values of $R_p \sim 800$ Å and $\Delta R_p \sim 200$ Å are given here for ^{75}As implantation at 100 keV into PPS.

For the low and intermediate energy implants, a Gaussian distribution of implants is expected [13], and this has been confirmed experimentally [4-6]. For example Auger electron spectroscopy has been used to measure the spatial profile of the implanted ions in a polymer. The results verify the Gaussian distribution, and the magnitudes of R_p and ΔR_p are consistent with LSS theory; specific results have been reported in terms of the arsenic Auger line at 376 eV for ^{75}As implanted into PAN at 200 keV to a fluence of $1.0 \times 10^{16}/cm^2$ [6]. In addition, Auger spectra for elements of the host polymer material have been measured and the results indicate a depletion of volatile components such as sulfur in PPS in the near-surface region ($d < R_p$) and a corresponding relative increase in carbon concentration in PPS implanted with ^{84}Kr at 100 keV and a fluence of $1 \times 10^{16}/cm^2$. In contrast to the Gaussian distributions discussed above for the low and intermediate energy ion implants, the ions completely penetrate the thin film samples ($1000 < d < 3000$ Å) implanted at high energies (E = 2 MeV) and high fluence [2,7,8].

Structural Damage and Chemical Modifications

Ion implantation damage to polymers tends to be more destructive and irreversible in comparison with other types of targets. Some polymers (particularly those with simple unbranched chains) tend to crosslink and conjugate, while others (especially those with complex side chains) tend to degrade. For a given implant, the type of implantation-induced structural damage and chemical modification depends sensitively on the ion energy and mass. The extent of the structural damage depends sensitively on the fluence. Specifically, larger ionization density along the track of a high mass ion results in much larger structural damage in the case of high mass ions compared to lower mass ions with comparable energy and fluence. Evidence for irreversible structural changes for intermediate and high energy implants is provided by a variety of techniques.

Of particular significance has been the monitoring of the gas evolution during the implantation process, using an in-situ residual gas analyzer (quadrupole mass spectrometer) within the ion implantation chamber. For the case of ^{80}Br implanted into PAN at 200 keV, large amounts of hydrogen gas are emitted during the implantation process [6] with a very large initial increase in gas evolution followed by a decrease

https://doi.org/10.1557/PROC-27-413 Published online by Cambridge University Press

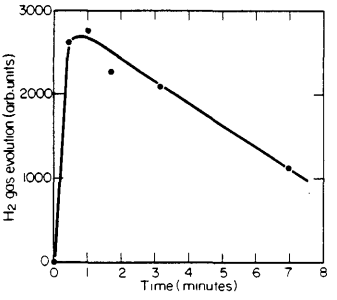

Fig. 2. Gas evolution of a polymer resulting from ion implantation. Here hydrogen gas evolution (arbitrary scale) is plotted as a function of time of implantation (proportional to ion fluence) obtained with an in-situ residual gas analyzer and a PAN film implanted with ^{80}Br at 200 keV.

at later times as shown in Fig. 2; here the time scale is proportional to the ion fluence. From the massive gas evolution we infer that the energy dissipation of the incident ions by the electronic energy loss mechanism occurs through the formation of large densities of free radicals (as confirmed by ESR measurements on the same samples [14]) and the molecular recombination of side chain and backbone constituents in the vicinity of free radical sites. We further infer that the implantation-induced structural changes result in conjugation of the polymer chains, the extent of the conjugation increasing with increasing ion energy. From Fig. 2, we see that as the fluence is initially increased, the gas evolution also increases, suggesting the release of loosely bound hydrogens from the sidechains. As diffusion proceeds, the gas evolution increases until a significant fraction of the hydrogens are removed, after which the probability of further gas evolution is reduced.

Copious gas evolution was also observed for high energy (2 MeV) implants into polymers. Massive quantities of CO_2, CO, formic acid, acetic acid and other species were detected by a quadrupole mass spectrometer [12] upon implantation of PMMA by 2 MeV ^{40}Ar ions. By monitoring the time dependence of the irradiation-induced emission using a 50 msec pulsed ion beam, and identifying the emission delays with molecular diffusion through the polymer films, a determination of the diffusion coefficients of various gases in polymers was made [12]. Radiation-enhanced oxidation commonly occurs in polymers such as $(CH)_x$, PPO and PVC [15].

For certain organic films (e.g., PTCDA), high energy, high fluence ion implantation is found to reduce the films mainly to carbon, with a large depletion of the original nitrogen content. These stoichiometric determinations were sensitively measured using Rutherford backscattering spectrometry (RBS) [8]. The RBS results are consistent with the copious gas evolution of volatile constituents in ion implanted PAN [6]. These stoichiometric modifications are also consistent with the shrinkage of the PTCDA film thickness from 3000 Å to 1500 Å upon ^{40}Ar implantation at 2 MeV and a fluence of $10^{16} cm^{-2}$ [8].

Even for low energy implants (e.g., 25 keV ^{106}Pd and ^{80}Br into $(CH)_x$), the broadening of the 1s carbon XPS (ESCA) lines indicates extensive structural damage. A comparison of the intensities of the 1s nitrogen ESCA peak with the 2p sulfur peak further indicates implantation-induced depletion of nitrogen in $(SN)_x$ in the near-surface region for low energy (25 keV) ^{80}Br ions at a fluence of $\phi = 5 \times 10^{15} cm^{-2}$ [9]. Evidence has also been presented for the chemical binding of the implanted bromine to a single site of the $(CH)_x$ backbone. Even for high fluences of implantation in the low energy regime, no evidence for implantation-induced ion diffusion was reported, based on RBS, ESCA, and infrared and ESR spectroscopies. From these measurements it is inferred that low energy implantation of ^{80}Br into $(CH)_x$ results in the formation of free radicals and some

https://doi.org/10.1557/PROC-27-413 Published online by Cambridge University Press

neutral hydrogen which is subsequently released as hydrogen gas, in addition to bonding some of the halogens to the polymer backbone.

Qualitative evidence for implantation-induced changes in the structure and properties of polymer targets is provided by color changes of the films upon implantation. For polymer films that are colorless prior to implantation, irradiation with the ion beam often imparts a brownish tinge upon implantation at low fluences. The color change deepens with increasing fluence and the effect is more pronounced for high energy implants. For example, PTCDA films exhibit a darkening for $\phi \geq 10^{12}cm^{-2}$; this darkening increases until a fluence of $5 \times 10^{15}cm^{-2}$ where the irradiated stripe was reported to become a dense shiny black. These color changes, the gas evolution and the stoichiometric changes all suggest the formation of carbonaceous material as a result of implantation of polymers. For high energy and high fluence implants (E = 2 MeV, $\phi \geq 10^{16}cm^{-2}$), evidence from the transport measurements described below suggest that this carbonaceous material bears a close resemblance to coal or amorphous carbon.

Electrical Conductivity

Dramatic increases in electrical conductivity σ (by 14 orders of magnitude) have been reported to result from ion implantation into a variety of normally insulating polymers and organic films under various conditions of implantation [4-8]. The general dependence of the conductivity on ion fluence ϕ seems to be qualitatively similar for several different ion species implanted into several host polymers under different implantation conditions. Examples of the observed dependence of log σ on log ϕ are shown in Fig. 3(a) for ^{84}Kr, ^{75}As and ^{80}Br into PPS [5] and in Fig. 3(b) for ^{40}Ar into various organic films [7,8]. Similar results have also been obtained for various implants into other polymers [6]. Measurements in all cases are made in the ohmic region; in Fig. 3(a), microelectronics devices (based on charge flow transistor technology) are used in the conductivity measurements, while the measurements in Fig. 3(b) were made with conventional 4-probe techniques, except for the high resistivity regime where 2-probe techniques had to be used.

For normally insulating polymers and organic films that can be made conductive by implantation, the lowest significant conductivity values shown in Fig. 3 ($\sim 10^{-9}$ to 10^{-10} $(\Omega cm)^{-1}$) correspond to a fluence of $\sim 10^{14}cm^{-2}$, where extensive structural modifications have already occurred, as indicated by optical transmission measurements [7,16]. While as-deposited organic films show a rich spectra of absorption bands, ion doses as low as $\phi \sim 10^{12}cm^{-2}$ are effective in attenuating and broadening absorption bands; at a fluence of $\sim 10^{14}cm^{-2}$ and above, a featureless absorption spectrum is obtained, suggesting the formation of amorphous carbon[7].

In the fluence range $10^{14} < \phi < 5 \times 10^{15}cm^{-2}$, a rapid increase in conductivity is observed, followed by a saturation behavior above $\sim 5 \times 10^{15}cm^{-2}$. It is significant that the behavior shown in Fig. 3 is common to a wide variety of implanted polymers over a similar fluence range. From these measurements we conclude that the dominant effect of ion implantation is the generation of defects such as scission and cross linking of polymers chains, the generation of broken bonds associated with the liberation of volatile species, and the formation of free radicals, double bonds and charge carriers. In the range $10^{14} < \phi < 5 \times 10^{15}$ cm^{-2}, chemical modifications to the polymer chains seem to be less important than the formation of structural defects, since little dependence on ion species is found. The results however suggest that the absolute magnitude of the conductivity achieved at the highest available fluences increases with increasing ion energy.

The correspondence of the maximum conductivity for the high energy implants with that of amorphous carbon suggests that ion implantation plays a role similar to high temperature heat treatment in the pyrolysis

https://doi.org/10.1557/PROC-27-413 Published online by Cambridge University Press

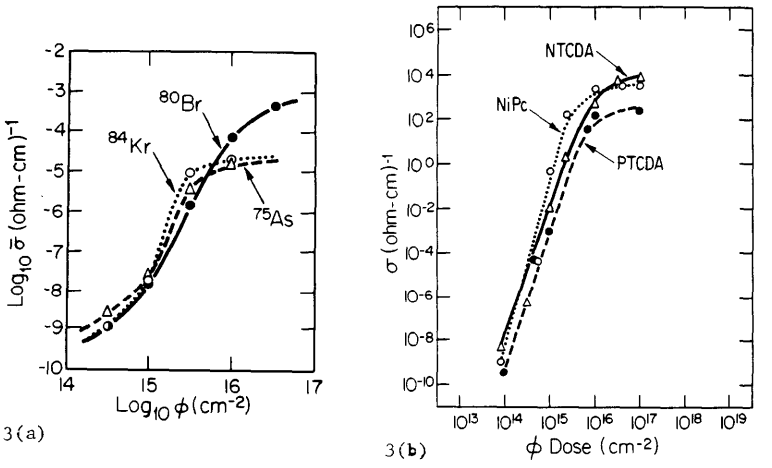

Fig. 3. Log-log plots of the dependence of the room temperature conductivity on the fluence of implantation. (a) Conductivity plot of ^{84}Kr (at 100 keV), ^{75}As (at 100 keV) and ^{80}Br (at 200 keV) implanted into PPS. (b) Resistivity plot of ^{40}Ar (at 2 MeV) implanted into PTCDA (closed circles), NTCDA (triangles) and NiPc (squares).

of precursor materials to form carbons. In this context, an analogy can be made between higher ion energies and higher heat treatment temperatures, so that as the incident ion energy is increased, the implantation process becomes more effective in selectively removing non-carbon atoms from the original polymer material. It is of interest to note that the maximum conductivity that has been achieved by ion implantation at high energies (2 MeV ^{40}Ar ions with $\phi \sim 10^{16}$ cm^{-2}) is at least an order of magnitude greater that for amorphous carbon [7], which implies that high energy ions promote conjugation and formation of local sp^2 carbon bonds. The higher graphitic content of the ion-implanted materials relative to amorphous carbon prepared by evaporation is also supported by the Raman spectra obtained from similar ion-implanted samples as were used for the conductivity measurements [2,7].

The rapid increase in conductivity with increasing ion fluence can also be related to other characterization measurements such as transmission electron microscopy (TEM) and electron spin resonance (ESR), discussed below. With regard to TEM measurements, sharp electron diffraction rings from as-deposited PTCDA films (indicating polycrystalline grain sizes ranging between 100 Å and 500 Å) were transformed by 2 MeV ^{40}Ar ions at a fluence of 1.0×10^{15} cm^{-2} into a broad diffraction ring, characteristic of amorphous carbon [7,8].

The saturation effect above 5×10^{15} cm^{-2} is very pronounced for chemically inert implants (e.g., ^{40}Ar and ^{84}Kr) and also for ^{75}As, while reactive halogens may continue to exhibit modest increases in conductivity at higher fluences. The different behaviors in the saturation region between the reactive halogen implants and the chemically inert implants suggest the formation of halogen bonds to the polymer side chains and backbones. A similar bonding arrangement for implanted halogens has been proposed [9] for halogens implanted $(CH)_x$ and $(SN)_x$.

Valuable information on the conduction mechanism is provided by studies of the temperature and frequency dependence of the ion-implanted

https://doi.org/10.1557/PROC-27-413 Published online by Cambridge University Press

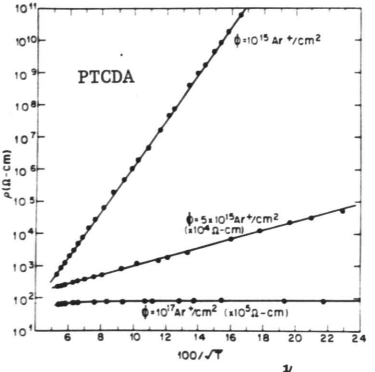

Fig. 4. Resistivity vs. $T^{-\frac{1}{2}}$ for 3000 Å PTCDA films at various doses of 2 MeV ^{40}Ar ions (from Ref. 7).

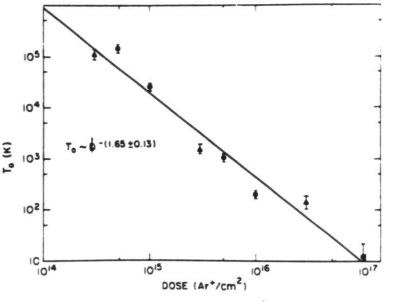

Fig. 5. Dependence of characteristic T_o vs. 2 MeV ^{40}Ar ion dose for PTCDA (circles) and NiPc (triangles) (from Ref. 7).

polymers. Measurements of the temperature dependence of the conductivity of the ion-implanted polymers PAN and PPO [6], PMMA and other photoresists [2] and of related organic films [7,8] all yield a functional form of $\sigma = \sigma_0 \exp(-T_0/T)^{\frac{1}{2}}$ for a wide range of fluences and energies of implantation (see Fig. 4). It is of interest to observe that the same functional form is applicable to a large number of different implants and polymers, and over a wide range of fluences [2,6-8], though the values of σ_o and T_o are strongly fluence dependent (see Fig. 5).

Two models have been used to interpret conductivity data in ion implanted polymers. A conducting grain model has been proposed by Forrest et al. [7] to explain the conductivity behavior for high energy implants. According to this model the polymer is considered to consist of conducting particles or grains (idealized as spheres) separated by narrow insulating regions [17] and the current is controlled by the quantum mechanical tunneling between the grains. The fluence dependence is related by percolation theory to the number of paths through the polymer. In the context of the charge grain model, the material is assumed to be uniform, consisting of conducting grains or islands which are identified with crystallites or with amorphous carbon particles of diameter d separated by nonconducting barriers of width w. According to this model, T_o becomes $T_o = 4\chi w E/k_B$ where $\chi = (2m^*\Psi/\hbar^2)^{\frac{1}{2}}$, and m^* is the effective mass, Ψ is the energy barrier height over which the charge must hop and E is the electrostatic energy necessary to remove a charge from an uncharged island and place it on an adjacent previously uncharged island, thereby producing two adjacent oppositely charged islands separated by a dielectric layer with permittivity η, so that assuming cylindrical symmetry, E is written as $E = 2q^2w/[\eta d^2(1/2 + (w/d))]$. From analysis of their data, Forrest et al. [7] determine w/d as a function of ϕ, and find for low fluences ($\phi \sim 10^{14}$ cm^{-2}), that (w/d) ~ 0.14, which they relate to conducting grains in the range 200 < d < 500 Å separated by w in the range 15 < w < 20 Å. With increasing ϕ, the w/d ratio is found to decrease as $\phi^{-0.83}$, so that for high fluences, w becomes less than the nearest neighbor interatomic distance, indicating the formation of bridges between conducting grains.

A one-dimensional hopping model has been proposed to explain transport phenomena in polymers implanted with ions of intermediate energies

https://doi.org/10.1557/PROC-27-413 Published online by Cambridge University Press

$50 < E < 250$ keV [6]. The H_2 gas evolution suggests that the saturated bonds along the polymer chains are broken by collision with the energetic ions, and double bonds, free radicals and free carriers are generated. However, a hopping mechanism is necessary to complete the conduction path through the bulk material, as implied by the transport measurements of Wasserman et al. [6] and summarized below. This model relates to conduction in the semiconducting chalcogenide glasses, which are built from helical chains of Se atoms, that become highly disordered by doping the Se with other elements, thereby modifying and breaking the chains. In the ion implanted polymers, the one-dimensional character of the material is identified with the disordered polymer chains, with charge transfer occurring via hopping along, across and between the chain fragments.

Since ion implanted polymers have a morphology similar to that of chalcogenide glasses, it is suggestive to apply models which have been developed for these materials to the ion implanted polymers. On the basis of the one-dimensional thermally activated hopping model, the conductivity is expected to follow the relation $\ln(\sigma/\sigma_o) = -(T_o/T)^{\frac{1}{2}}$, in agreement with experimental results on ion implanted polymers. The model defines T_o by $T_o = 4\alpha/k_B N(E_F)$, where α denotes the exponential decay of localized states, k_B is the Boltzmann constant and $N(E_F)$ the density of states at the Fermi energy.

According to this one-dimensional variable range hopping model, a significant frequency dependence is expected. The frequency dependence of the real part of the conductivity is normally written in the form $\sigma_\omega = \sigma_o + A\omega^s$. For the charged grain model s is expected to be between $0.8 \leq s \leq 1$, while the experimental results [6] indicate a frequency dependent s rising above $s \approx 2$ for $\omega \geq 50$ kHz in PAN implanted with 200 keV ^{80}Br ions to a fluence of 2×10^{16} cm^{-2}. For the one-dimensional variable range hopping model a frequency dependence of $(\omega \ln\omega)^2$ is predicted [18]. Thus the frequency dependent conductivity appears to favor the one-dimensional variable range hopping model, though much quantitative work remains to be done.

DISCUSSION

Other transport and related measurements, such as thermoelectric power, Hall effect, optical transmission and electron spin resonance (ESR) also relate to the conduction mechanism. A summary of results obtained with these techniques is given here and related to the conduction model.

The temperature dependent thermopower measurements on ion implanted PAN and PPO exhibit the form $S = S_o + \beta T$ which is consistent with the one-dimensional variable range hopping model [6]. For example for PAN implanted with ^{80}Br to a fluence of 2×10^{16} cm^{-2}, n-type behavior is found with $S_o = -2.4\mu V/K$ and $\beta = 0.018\ \mu V/K^2$ for temperatures $200 < T < 300$ K. The small magnitude of the thermopower implies a large carrier density of very low mobility carriers [6]. A lower limit on the carrier mobility μ is found from attempted Hall effect measurements on the same sample as for the thermoelectric power, yielding $\mu \leq 10^{-3}$ cm^2/V sec [16]. Very low mobilities are also characteristic of chalcogenide glasses.

Important information relevant to the conduction process in ion implanted polymers has also been obtained from analysis of the visible spectra of PPO and PPS in the wavelength range $310 < \lambda < 850$ nm [16]. The results show a slowly increasing absorption with a nearly exponential dependence near the absorption edge. The short wavelength portion of the spectra can be interpreted in terms of a plasma resonance absorption which is fitted to obtain an estimate for the carrier density. An approximation to Mie's general formula for light scattering by small particles has been given by Kawabata and Kubo [19] where the transmission coefficient γ is related to the plasma resonance wavelength λ_R by the Lorentzian form

https://doi.org/10.1557/PROC-27-413 Published online by Cambridge University Press

$\gamma = \gamma_o\varepsilon_2/[\beta^2(\lambda-\lambda_R)^2+\varepsilon_2^2]$ where $\gamma_o = 18\pi\alpha(\varepsilon_m^3)^{\frac{1}{2}}/\lambda_R$ in which α is the volume density of the conductive part of the sample, ε_m is the dielectric constant of the non-conducting medium in which the conducting particles are embedded, ε_1 and ε_2 are the real and imaginary parts of the measured dielectric constant and β is the dispersion $\beta = \partial\varepsilon_1/\partial\lambda$ near the resonant wavelength λ_R. A good fit to this Lorentzian function for γ has been obtained for PPO implanted with 1 x 10^{16} cm^{-2} ^{80}Br ions at 200 keV for the wavelength range 310 < λ < 730 nm. A small deviation at higher wavelengths is attributed to the exponential shape expected near the absorption edge of disordered materials (Urbach rule [20]). The analysis carried out to relate the carrier density to λ_R employs the Bruggeman effective medium theory [21] by which λ_R and the bulk plasma frequency ω_p are related by $\lambda_R = 2\pi c/\omega_p^*$ where $\omega_p^* = (\{\omega_p^2/f\}-\tau^{-2})^{\frac{1}{2}}$ and $f = 1 + n^2(2+\alpha)/(1-\alpha)$ and $\varepsilon_2(\lambda_R) = [f\lambda_R/\pi\tau c]$ where n is the refractive index, τ is the scattering time and α is the volume density of the conducting medium. The analysis of the transmission data yields an estimate of the carrier density (~3.5 x $10^{22}/cm^3$) and an estimate for the length of the dipole moment (~5 Å) responsible for free carrier optical absorption. Qualitatively, the broadness of the Lorentzian lineshape suggests a very short dipole moment which is readily interpreted by the one-dimensional variable range hopping model in terms of long thin charged particles (chains) with short lateral separations (interchain distances). In contrast, it is difficult to explain the broad Lorentzian lineshape in terms of a charge grain model.

Information on the density of free radicals and free carriers is provided by ESR measurements carried out on similar polymer samples [14]. In contrast to the absence of any ESR signal for the unimplanted polymers, the implanted polymers show a single, narrow Lorentzian ESR line, indicative of homogeneous broadening and non-metallic behavior, consistent with the conductivity model described above. As the fluence is increased, the ESR linewidth is observed to decrease, indicating motional narrowing and an increased delocalization of the carriers along the polymer chains. The decrease in the ESR linewidth $\Delta\omega$ with increasing ϕ indicates the formation of C=C double bonds [22] to a density n_d where $\Delta\omega \sim (n_d)^{\frac{1}{2}}$. The ϕ dependence of the ESR signal intensity shows a rapid increase up to a fluence of ~5 x 10^{15} cm^{-2} above which saturation is observed. It is significant that a similar behavior for the ESR signal intensity is found for both PAN and PPO and that the saturation behavior for the ESR signal and conductivity occur at the same fluence, suggesting an overlap in carrier wavefunctions between adjacent chains in this limit.

To separate the contribution of the localized spins (free radicals) and conduction electrons, the temperature dependence of the ESR signal was investigated in the range 90 < T < 300 K [14]. Since the density of localized spins n_s follows a Curie law, while the density of free carriers n_f make a temperature-independent Pauli contribution to the ESR signal intensity, by fitting the temperature dependence of the ESR intensity n_s and n_f can be separately determined. Investigation of the temperature dependent ESR signal intensity for a range of fluences for a variety of implanted PPO and PAN samples shows that for low fluences (~6 x 10^{14} cm^{-2}) the density of free carriers is about an order of magnitude smaller than the density of free radicals, while at high fluences (~1 x 10^{16} cm^{-2}), the densities of free carriers and free radicals are about equal [14].

The total density of spins in PPO implanted with 200 keV ^{80}Br ions is found to be 6 x 10^{17} spins/g (for ϕ = 6 x 10^{14} cm^{-2}) and 2.7 x 10^{19} spins/g (for ϕ = 1 x 10^{16} cm^{-2}). Taking into account the mass density of the polymer film (~3) and the fraction of the ~2 μm film that contains unpaired spins (~1/7) leads to a rough estimate of ~5 x 10^{20} spins/cm^3 for PPO implanted to 10^{16} cm^{-2} with 200 keV ^{80}Br ions. A comparison of this spin density with the carrier density deduced from the optical transmission data suggests that only a fraction of these carriers have unpaired

spins [14]. Although the one-dimensional variable range hopping model account for many of the observed phenomena, many questions about the nature of the charge transport in ion implanted polymers remain unanswered.

ACKNOWLEDGMENTS

We gratefully acknowledge Drs. K. Sugihara, T. Venkatesan and G. Dresselhaus for many discussions, and the NSF-MRL grant #DMR-81-19295 for support.

REFERENCES

1. B.S. Elman, M.S. Dresselhaus, G. Braunstein, G. Dresselhaus, T. Venkatesan, B. Wilkens, and J.M. Gibson, Proceedings of this Symposium.
2. T. Venkatesan, S.R. Forrest, M.L. Kaplan, C.A. Murray, P.H. Schmidt, and B.J. Wilkens, J. Appl. Phys. 54, 3150 (1983).
3. T.M. Hall, A. Wagner and L.F. Thompson, J. Appl. Phys. 53, 3997 (1982).
4. J.S. Abel, H. Mazurek, D. R. Day, E.W. Maby, S.D. Senturia, G. Dresselhaus, and M.S. Dresselhaus, in Metastable Materials Formation by Ion Implantation, Proceedings of the MRS Symposium on Ion Implantation, edited by S.T. Picraux and W.J. Choyke, North Holland, New York 1982, Vol. 7, p. 173.
5. H. Mazurek, D.R. Day, E.W. Maby, J.S. Abel, S.D. Senturia, G. Dresselhaus, and M.S. Dresselhaus, J. Polymer Science, Polymer Physics Edition 21, 539 (1983).
6. B. Wasserman, M.S. Dresselhaus and G. Wnek, Proceedings of this Symposium.
7. S.R. Forrest, M.L. Kaplan, P.H. Schmidt, T. Venkatesan, and A.J. Lovinger, Appl. Phys. Lett. 41, 708 (1982).
8. M.L. Kaplan, S.R. Forrest, P.H. Schmidt, T. Venkatesan and A.J. Lovinger (unpublished).
9. W.N. Allen, P. Brant, C.A. Carosella, J.J. DeCorpo, C.T. Ewing, F.E. Saalfeld, and D.C. Weber, Synthetic Metals 1, 151 (1980).
10. D.C. Weber, P. Brant, C.A. Carosella, L.G. Banks, J.C.S. Chem. Commun. 198, 522 (1981).
11. D.C. Weber, P. Brant, and C.A. Carosella, in Metastable Materials Formation by Ion Implantation, Proceedings of the MRS Symposium on Ion Implantation, edited by S.T. Picraux and W.J. Choyke, North Holland, New York 1982, Vol. 7, p. 173.
12. T. Venkatesan, W.L. Brown, C.A. Murray, K.J. Marcantonio, and B.J. Wilkins (unpublished); T. Venkatesan, D. Edelson and W.L. Brown (unpublished).
13. J. Lindhard, M. Scharff, H.E. Schiott, Mat. Fys. Medd. Dan. Vid. Selsk. 33, 14 (1963).
14. G.E. Wnek, I.-H. Loh and B. Wasserman, (to be published).
15. M.C. Wintersgill, 2nd Int. Conf. on Radiation Effects in Insulators, Albuquerque, NM (1983) p. 92.
16. B. Wasserman (unpublished).
17. P. Sheng, B. Abeles and Y. Arie, Phys. Rev. Lett. 31, 44 (1973); B. Abeles, P. Sheng, M.D. Coutts, and Y. Arie, Adv. in Phys. 24, 407 (1975).
18. A.A. Gogolin, Physics Reports 86, 1 (1982).
19. A. Kawabata and R. Kubo, J. Phys. Soc. Jpn. 21, 284 (1966).
20. N.F. Mott and E.A. Davis, Electronic Processes in Non-Crystalline Materials, (Clarendon Press, Oxford, 1979) p. 287-293.
21. Y.K. Szeto, BS Thesis, Univ. of Toronto, 1980 (unpublished); R. Landauer, AIP Conference Proceedings, No. 40, edited by J.C. Garland and D.B. Tanner, American Institute of Physics (1978), p. 2.
22. S. Onishi, Y. Ikeda, S. Sugimoto and I. Nitta, J. Polymer Science 47, 503 (1960).